

## A high performance PZT ribbon-based nanogenerator using graphene transparent electrodes

Junggou Kwon,<sup>†</sup> Wanchul Seung,<sup>†</sup> Bhupendra K. Sharma, Sang-Woo Kim\* and Jong-Hyun Ahn\*

Received 17th May 2012, Accepted 6th July 2012

DOI: 10.1039/c2ee22251e

We report a simple and effective approach for high performance  $\text{PbZr}_{0.52}\text{Ti}_{0.48}\text{O}_3$  (PZT) based flexible and semi-transparent NGs that exploit the electrical, mechanical and transparent properties of graphene. PZT NGs are successfully demonstrated for continuous driving of a liquid crystal display screen and a light emitting diode. A good quality PZT film was deposited on Pt/Ti/SiO<sub>2</sub>/Si wafer by the sol-gel method, exhibiting a typical hysteresis loop in the low voltage region. A graphene film was used in the interdigitated electrode form to improve the PZT/graphene interface under mechanical stress. Further improvement in NGs performance was realized by p-type doping in graphene, resulting in an increase in current density. NGs showed a high output voltage  $\sim 2$  V, current density  $\sim 2.2 \mu\text{A cm}^{-2}$  and power density  $\sim 88 \text{ mW cm}^{-3}$  at an applying force of 0.9 kgf. This can efficiently run commercially available electronic components in a self-powered mode, without any external electrical supply.

### 1. Introduction

Energy harvesting has attracted a great deal of attention, because this type of technology could enable a variety of new applications, ranging from portable devices to implantable biosensors.<sup>1–6</sup> For these systems, various one-dimensional piezoelectric semiconductor materials ranging from zinc oxide and gallium nitride to cadmium sulfide represent an ideal choice, as demonstrated in various prototype devices.<sup>7–16</sup> Integration of flexibility to a nanogenerator has received increasing interest for realizing the energy harvesting systems in practical life. Recently, ZnO nanomaterial based and tribological process based flexible nanogenerators have been demonstrated.<sup>17,18</sup> As for materials with electromechanical coupling,  $\text{PbZr}_{0.52}\text{Ti}_{0.48}\text{O}_3$  (PZT) is a good traditional piezoelectric material with a larger piezoelectric constant, as compared to those of piezoelectric semiconductor

materials. Therefore, there have been many approaches for development of high-performance piezoelectric energy harvesters based on PZT in bulk or thin film forms. Recent work explores a different approach that uses a direct printing of high-quality, bulk inorganic piezoelectric thin films on the wafers onto plastic substrates, to produce nanogenerators with high performance.<sup>19–21</sup> This method based on “top-down” techniques, including photolithographic patterning and etching of source wafers, has attracted much attention, because of the gain of higher voltage and power outputs, and the possibility of large area device fabrication using well-developed printing technologies. However, the short life-time, due to the poor mechanical properties of inorganic piezoelectric materials, has limited their practical applications, in spite of their high output voltage generation. Moreover, the opaque nature of these materials is a significant hurdle to apply these nanogenerators to new future applications that require optical transparency, such as nanogenerator embedded touch screens and wearable skin sensors.

In this work, we report high efficiency, semi-transparent PZT nanogenerators integrated with graphene films that possess outstanding mechanical and optical properties that can offer

SKKU Advanced Institute of Nanotechnology (SAINT) and Center for Human Interface Nano Technology (HINT), School of Advanced Materials Science and Engineering, Sungkyunkwan University, Suwon 440-746, Korea. E-mail: ahnj@skku.edu; kimsw1@skku.edu

<sup>†</sup> J. Kwon and W. Seung contributed equally to this work.

### Broader context

High performance  $\text{PbZr}_{0.52}\text{Ti}_{0.48}\text{O}_3$  (PZT)-based flexible semi-transparent piezoelectric nanogenerators that exploit the electrical, mechanical, and transparent properties of graphene have been developed. A good quality PZT film was deposited on Pt/Ti/SiO<sub>2</sub>/Si wafer by the sol-gel method, exhibiting a typical hysteresis loop in the low voltage region. A graphene film was used in the interdigitated electrode form to improve the PZT/graphene interface under mechanical stress. Further improvement in nanogenerator performance was realized by p-type doping in graphene, resulting in an increase in current density. For its practical applications, a liquid crystal display and a light emitting diode were driven by the piezoelectric output power without any external electrical supply.

unique benefits in high-performance flexible and transparent devices. All device components, including piezoelectric materials and graphene electrodes, were printed onto a plastic substrate, using a low temperature transfer process. The resulting graphene based PZT nanogenerator exhibits several advantages, such as good mechanical bendability, optical transmittance and simple device design, that are compatible with conventional batch fabrication steps, such compatibility is essential for realizing practical devices and systems.

## 2. Experimental section

The PZT thin film was deposited on Pt/Ti/SiO<sub>2</sub>/Si by the sol-gel method. A PZT solution gel of 0.4 M was prepared using lead acetate trihydrate, titanium-isopropoxide and zirconium-*n*-propoxide, with an ~48/52 composition ratio of Ti/Zr. The prepared gel was spin-coated (4000 rpm, 20 s) repeatedly 6 times on a Pt (150 nm)/Ti (10 nm)/SiO<sub>2</sub> (300 nm)/Si wafer, and after each coating, baking was done at 300 °C for 5 minutes. Finally the PZT film was annealed at 650 °C for 30 minutes to crystallize it. PZT ribbons were patterned using the conventional photolithographic method, followed by etching of Pt/Ti/SiO<sub>2</sub>/Si multi-layers. PZT was etched out by diluted HF solution, and Pt, Ti and SiO<sub>2</sub> layers were etched out by inductively coupled reactive ion etching, using Ar, Cl<sub>2</sub>, and CHF<sub>3</sub> gases, respectively. Lateral etching of Si was carried out by a XeF<sub>4</sub> dry method. After etching, PZT ribbons were transferred to the NOA coated polyethylene terephthalate (PET) flexible substrate with the help of a PDMS stamp. For electrodes, instead of using a traditional metal, graphene sheets were patterned on PZT ribbons. Graphene sheets for electrodes were grown on Cu foil by the CVD method. Cu foils in a tubular quartz tube of a CVD system were heated up to 1000 °C, with 10 sccm flow of H<sub>2</sub> gas at a pressure of 80 mTorr for 30 min. In the growth step, the precursor gas CH<sub>4</sub> (15 sccm) was injected at a pressure of around 1.6 Torr for 30 min. After this step, the Cu foils were rapidly cooled down to room temperature. This CVD process produced the graphene film with a high quality monolayer coverage of over 95%. To form the multi-layered graphene film, poly(methyl methacrylate) (PMMA) was coated on graphene/Cu foil. After etching the Cu by ammonium persulfate (APS) solution, the PMMA-graphene film was transferred to another graphene-Cu foil. When the desired number of stacks was produced, it was transferred onto plastic substrates. The PMMA support was effectively removed using boiled acetone up to 80 °C.

## 3. Results and discussion

A PZT thin film of thickness ~500 nm was deposited on Pt/Ti coated SiO<sub>2</sub>/Si wafer using the sol-gel method. The sol-gel method offers various advantages, including cost effectiveness, scalability, low residual stress, and easy processing and tuning of the desired chemical composition, compared with other processes. Cross-sectional views of the as deposited multi-layers (PZT/Pt/Ti/SiO<sub>2</sub>/Si) were confirmed by scanning electron microscopy (Fig. 1a), and crystalline quality was investigated using the X-ray diffraction pattern (inset of Fig. 1a). The advantage of depositing the PZT thin film over a Pt/Ti layer is to get good crystallization of PZT, as under high temperature annealing (550–800 °C), the diffusion of Ti into and through Pt

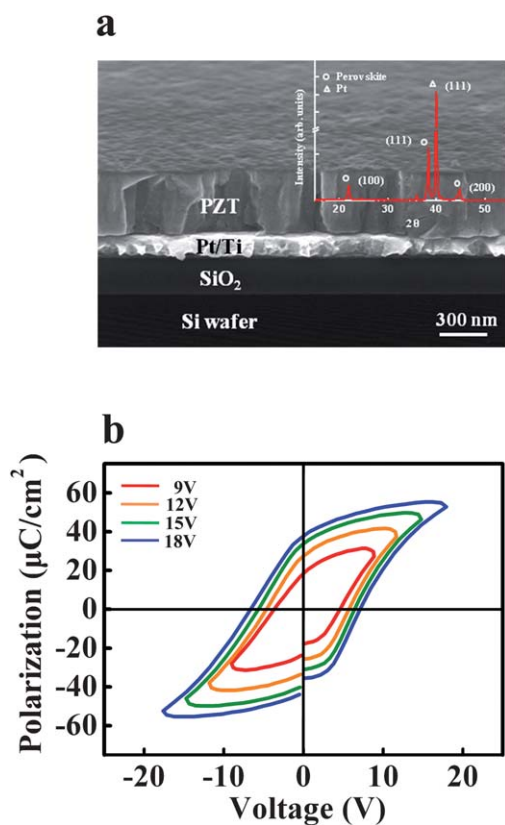


**Fig. 1** Structural characterization of PZT. (a) Scanning electron microscopy (SEM) image of the PZT film deposited on Pt/Ti/SiO<sub>2</sub>/Si wafer. The inset shows XRD patterns of the PZT thin film prepared through the sol-gel process. (b) Polarization hysteresis loop of the PZT film at different applied voltages.

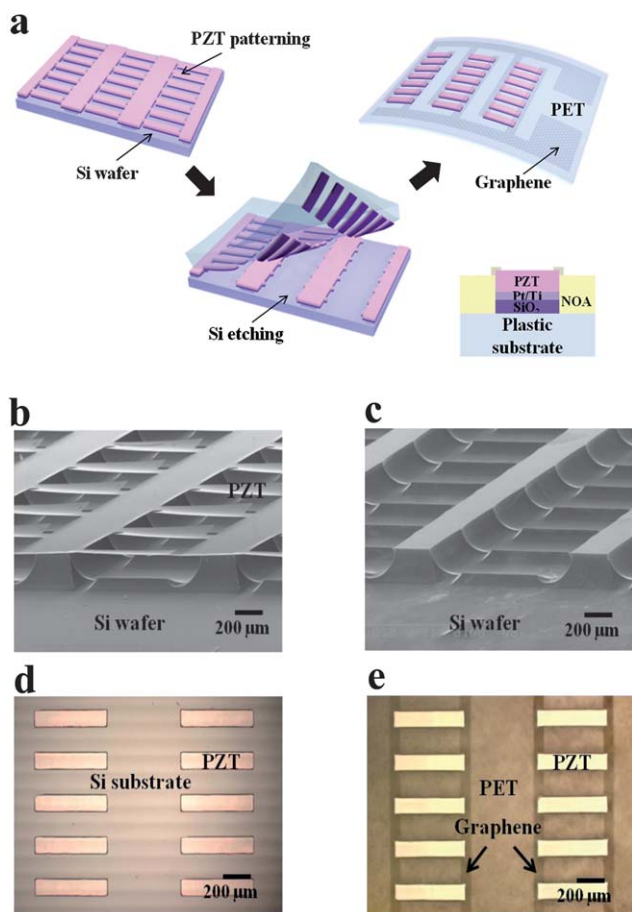
leads to the formation of the Pt<sub>3</sub>Ti compound, which helps to crystallize the perovskite PZT phase.<sup>22</sup> X-ray diffraction of the PZT film clearly indicated that the PZT film is highly textured along the (111) orientation, which is good in that it has high remanent polarization. The crystallographic phase of the PZT film depends on the internal composition of Ti:Zr and the annealing temperature. In the present study, we used a 48/52 ratio for Ti/Zr, which is known as the morphotropic phase boundary, *i.e.* tetrahedral and rhombohedral phases coexist metastably after high temperature treatment, and provide good electromechanical efficiency.<sup>23,24</sup> The polarizing properties of the as-deposited PZT thin film were studied by measuring the hysteresis loop ( $P$ - $V$  curve) with respect to a different voltage sweeping range (Fig. 1b). Hysteresis loops were found to be symmetric, and showed an increase in remanent polarization ( $P_r$ ) with increasing sweeping range of applied voltages. The remanent polarization ( $P_r$ ) increases from 17  $\mu\text{C cm}^{-2}$  at  $\pm 9$  V to 43  $\mu\text{C cm}^{-2}$  at  $\pm 17.5$  V sweeping ranges, indicating that a well-saturated hysteresis loop with high remanent polarization could be achieved from the as-deposited PZT thin film, even at a low applied voltage range. After confirming the good quality of the PZT thin film on Si wafer, we used it for further fabrication of the PZT based nanogenerators (NGs).

Fig. 2a depicts the schematics of various steps during the fabrication of PZT ribbon-based NGs on a PET film. First,

PZT/Pt/Ti/SiO<sub>2</sub> ribbons with the desired size of 500 μm × 100 μm were created using the conventional photolithographic method (Fig. 2a, first step). After that, an open area of PZT was created, and below it Pt/Ti, SiO<sub>2</sub> and then lateral etching of Si layers was carried out sequentially. PZT was etched out by diluted HF solution, and Pt/Ti and SiO<sub>2</sub> layers were etched out by inductively coupled reactive ion etching. Lateral etching of Si was carried out by a XeF<sub>4</sub> dry method. After completing the etching, PZT/Pt/Ti/SiO<sub>2</sub> ribbons on the Si substrate were laminated by PDMS stamp, and detached (Fig. 2a, second step). The behavior of the etching process and the complete removal of ribbons were confirmed by cross-sectional SEM view of PZT/Pt/Ti/SiO<sub>2</sub>/Si after partial etching, and of the bare Si substrate after detaching the ribbons, as shown in Fig. 2b and c, respectively. Fig. 2d shows the optical image of PZT ribbons after etching on the Si substrate. An adhesive layer, Norland optical adhesive (NOA), was spin coated on the PET film, and attached to a PZT/Pt/Ti/SiO<sub>2</sub> laminated PDMS stamp attached with NOA coated PET was cured with UV light, and then detached carefully in order to transfer the ribbons onto the

PET film. The NOA adhesive layer helps to level the surface of device substrates and improve the adhesion of ribbons to the plastic substrate. Next, graphene films grown by the CVD method were transferred to the top of PZT ribbons, and patterned as interdigitated electrodes to transport harvested electrons, as shown in Fig. 2a, third step. An optical image of the transferred PZT ribbons on the PET film with patterned graphene based interdigitated electrodes is shown in Fig. 2e, which indicates that the ribbons are well aligned, without destroying their orientation and cracking.

The key features of graphene electrodes enable optically transparent and flexible nanogenerators, due to their great mechanical and optical properties. However, the low conductivity of pristine graphene can limit the performance of the resulting devices. To overcome these disadvantages of graphene, we used a multilayer stacking method, and chemical doping with p-type dopant HNO<sub>3</sub>, which resulted in improved performance of the devices. The doping effect in graphene films was characterized by Raman spectroscopy (Fig. 3a–c) and the sheet resistance was measured (Fig. 3d). The 'G' and '2D' peaks were found to have shifted from 1580 cm<sup>-1</sup> to 1587 cm<sup>-1</sup> and 2685 cm<sup>-1</sup> to 2692 cm<sup>-1</sup> respectively, whereas the intensity ratio  $I_{2D}/I_G$  increases after the doping. The sheet resistance was found to decrease drastically, from 133.34 Ω per sq to 49.95 Ω per sq (62%), after HNO<sub>3</sub> doping in graphene films. Fig. 4a shows a photograph of the as-fabricated PZT based NGs on the PET film with printed text as background, to demonstrate their optical transmittance and mechanical bendability. Optical transmission spectra of PZT NGs integrated on the PET film and bare graphene films in the visible range are shown in Fig. 4b. The average transmittance through the PZT ribbons combined with graphene electrodes was observed to be ~67.2% (blue line), and for bare



**Fig. 2** Schematic illustration of the fabrication steps of a flexible PZT nanogenerator with graphene electrodes and optical images. (a) Overview of the fabrication process for PZT NGs and schematic cross-sectional view. (b) PZT nanoribbons after the lateral etching of the sacrificial layer, silicon. (c) The silicon wafer after the PZT nanoribbons were transferred. (d) Optical image of PZT nanoribbons on silicon wafer. (e) PZT nanoribbons with graphene electrodes on the PET film.

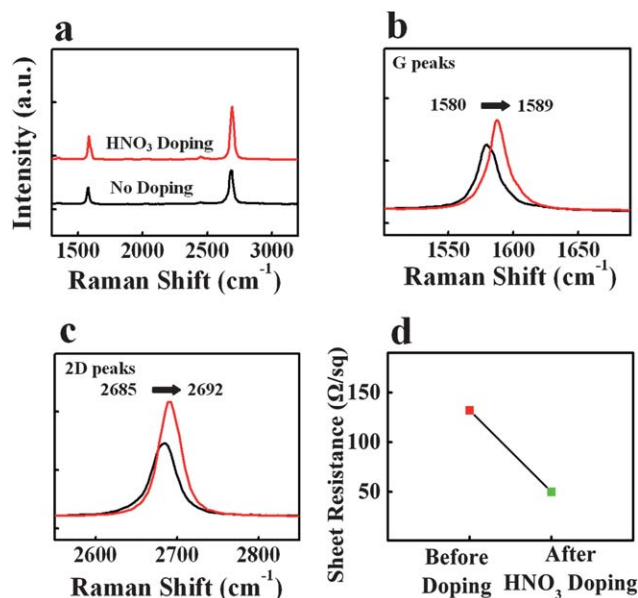


**Fig. 3** (a) Raman spectra of HNO<sub>3</sub> doped (top) and pristine (bottom) four-layer graphene films. (b and c) Raman spectra of HNO<sub>3</sub>-doped graphene films, showing ~7 cm<sup>-1</sup> redshift both for G and 2D peaks. (d) Sheet resistance measurement of graphene films before and after HNO<sub>3</sub> doping, showing ~28% change.

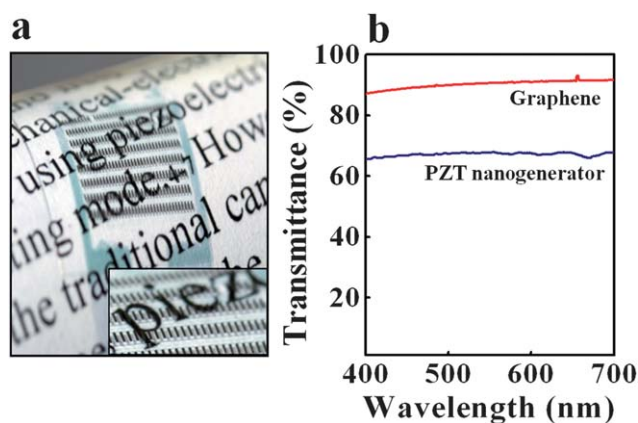


**Fig. 4** Images and transmission spectra of printed, semitransparent PZT arrays and graphene electrodes. (a) Images of transferred PZT ribbon arrays on NOA coated polyethylene terephthalate substrates. (b) Transmittance of the transferred PZT ribbons with graphene electrodes.

graphene films it was observed to be  $\sim 90.3\%$  (red line). The observed low value of transmittance for four layer graphene films is reasonable, as monolayer graphene decreases the transmittance by a factor of 2.3%.

To investigate the performance of the PZT ribbon-based flexible NGs, a nanovoltmeter and a picoammeter were used to detect the voltage and current output signals, respectively, generated from the device in response to the external mechanical force. Fig. 5a and b show the voltage and current response, respectively, of NGs when they are subjected to the cyclic compressive/releasing external force with respect to time. The generated voltage was measured at an average of  $\sim 2$  V and the current density was measured to be  $\sim 2 \mu\text{A cm}^{-2}$ . We have also investigated the change in voltage and current outputs with respect to time, by continuously increasing the compressive force in three steps, as shown in Fig. 5c and d. We observed that the generated voltage and current outputs increase with increasing compressive force as expected, because more pushing force creates more piezoelectricity in PZT ribbons. The generated voltage outputs were found to be  $\sim 1.0$  V,  $1.5$  V and  $2$  V, corresponding to  $0.3 \pm 0.02$  kgf,  $0.6 \pm 0.02$  kgf and  $0.9 \pm 0.02$  kgf applied forces, respectively, and current outputs were increased almost linearly from  $1 \mu\text{A cm}^{-2}$  to  $2 \mu\text{A cm}^{-2}$  (Fig. 5c and d). In addition, the device exhibits good stability, even after 7 days of testing (Fig. 5e). To get a significant polarization, PZT ribbons are polled in a strong electric field at below the Curie temperature, by applying the voltage between graphene interdigitated electrodes. During the testing of devices, an external mechanical stress applied on the top surface resulted in nonuniform charge distribution by displacing the positive–negative charge centers in PZT ribbons. This generates an overall net charge of opposite nature at the PZT/graphene interfaces, and these charges are further harvested by interdigitated graphene electrodes, resulting in output voltage and current signals. When the external mechanical stress is released, charge carriers start to flow in the reverse direction, resulting in negative voltage and current distribution (Fig. 5a and b), and piezopotential vanishes. The different values of voltage and current outputs in positive and negative distribution are possibly due to the different rates of force adopted by devices during the applying and releasing stages.

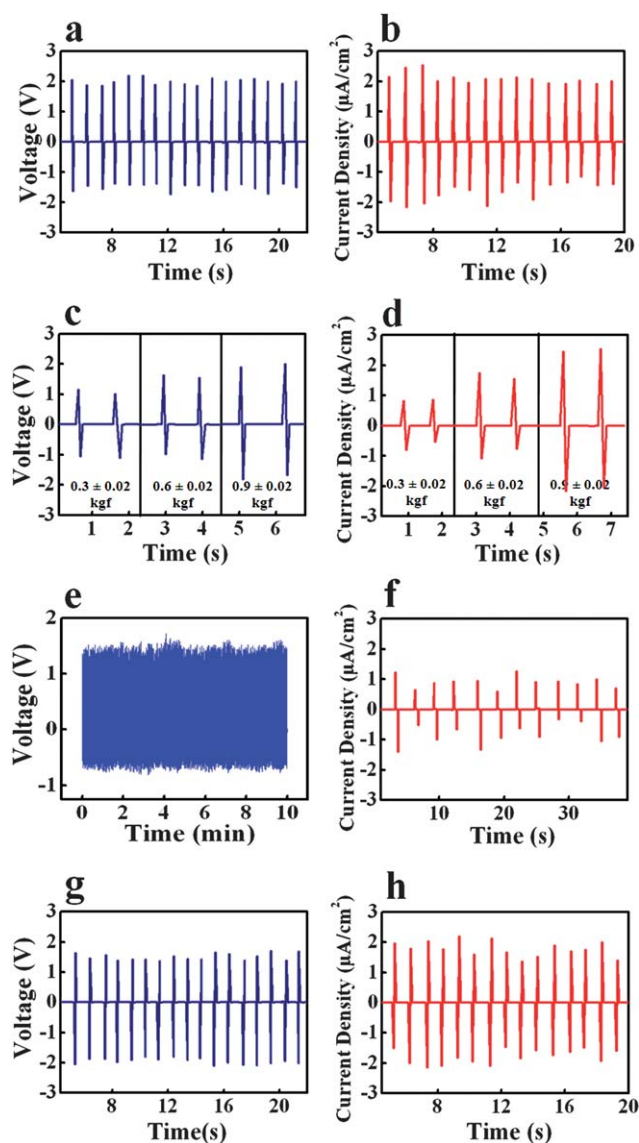


**Fig. 5** Output measurement of a PZT nanogenerator. (a) The voltage and (b) current density of a PZT nanogenerator with doped graphene electrodes when a dynamic load was applied on top of the generator by touch. (c) Different voltage and (d) current density signals were observed, depending on the pressure by touch. (e) Result of the durability test on the output of the PZT nanogenerator. The magnitude does not show any appreciable decay after 7 days for 10 minutes operation, showing good stability and robustness of the PZT nanogenerator. (f) Current density of the PZT nanogenerator with pristine graphene electrodes. (g) Output voltage and (h) current density in switching-polarity tests.

To confirm that the measured output signals were generated from PZT NGs, rather than from the measuring system, ‘switching polarity’ tests were also carried out. As we reverse the polarity of voltage and current meters, the output signals are reversed (Fig. 5g and h), maintaining the same value. The piezopotential generated from PZT ribbons can be estimated by the following relation:<sup>25</sup>

$$\Delta V = \int_0^1 g_{33} \sigma(l) dl$$

where  $l$  is the length of the ribbon between two interdigitated graphene electrodes,  $\sigma(l)$  is the stress function, and  $g_{33}$  is the piezoelectric voltage constant. By considering the PZT bulk value for  $g_{33}$  ( $0.025 \text{ V m N}^{-1}$ ),<sup>26</sup> the calculated piezopotential differs by 7.14% as compared to the measured one, for a maximum applied force of  $\sim 0.9 \text{ kgf}$ . The strain value developed in PZT ribbons for the external mechanical force of  $\sim 0.9 \text{ kgf}$  was also calculated, using the following equation:

$$\varepsilon_p = V_o / l_p E_p g_{33p}$$

where  $\varepsilon_p$  is the strain developed in PZT ribbon,  $l_p$  is the length,  $E_p$  is the modulus, and  $V_o$  is the observed voltage,  $\sim 2 \text{ V}$ . The calculated strain value was found to be  $\sim 4.0 \times 10^{-4}\%$ . The performance of NGs depends on the choice of electrodes and their electrical properties in response to repeated external mechanical stress. In the present study, the choice of graphene electrodes for harvesting the generated charges not only facilitates the fabrication of flexible NGs, but also maintains the PZT/graphene interface region during the repeated external mechanical force that can generate the cracks in any conventional metal. Further, the improvement in the performance of PZT ribbon-based NGs was realized by p-type ( $\text{HNO}_3$ ) doping in graphene. The output current density for doped graphene was found to be enhanced significantly, by nearly 2 times, as compared to the pristine one (Fig. 5f). Doping in graphene results in a change in sheet resistance, depending on the type of dopant and its concentration, as studied in our earlier reports.<sup>27</sup> The observed enhancement of current density in PZT NGs using doped graphene as electrodes can be attributed to its lower sheet resistance. When we apply a force on NGs vertically downwards, then the piezopotential develops opposite to the direction of the polling field. But this is not enough to reverse the alignment of dipoles, as the polling field was much higher than the developed piezopotential. So we require a relatively higher voltage to suppress the remanent polarization. As a consequence of mechanical pressure on NGs downwards, charges at interfaces are harvested through the interdigitated electrodes, leading to piezopotential across the electrodes. PZT ribbon-based NGs in the present study showed a higher voltage output ( $\sim 2.0 \text{ V}$ ), as compared to an earlier recently reported value ( $\sim 1.6 \text{ V}$ ) based on PZT nanofibers.<sup>28</sup> This may possibly be due to nanofibres being randomly aligned, causing degradation in net polarization and developing relatively less piezopotential under external mechanical stress. In addition, the present study demonstrates the successful integration of graphene electrodes that maintain the interface quality during repeated external mechanical stress and enhance device durability.

To realize the practical applications of as-fabricated PZT NGs, a liquid crystal display (LCD) was driven directly by its output power. An LCD screen with the Sungkyunkwan University logo was used for the test, and was directly connected to the output of NGs without any capacitor. Fig. 6a and b show the images of the snapshot taken before and after the LCD screen was turned 'ON', when the output power generated by the NGs exceeds the threshold voltage of the LCD screen. The output voltage and current density of the PZT NGs were measured at  $2 \text{ V}$  and  $2 \mu\text{A cm}^{-2}$  respectively. Thus, the LCD screen turned 'ON', by changing its color to black, when the PZT NGs were periodically mechanically stressed. In principle, the liquid crystal

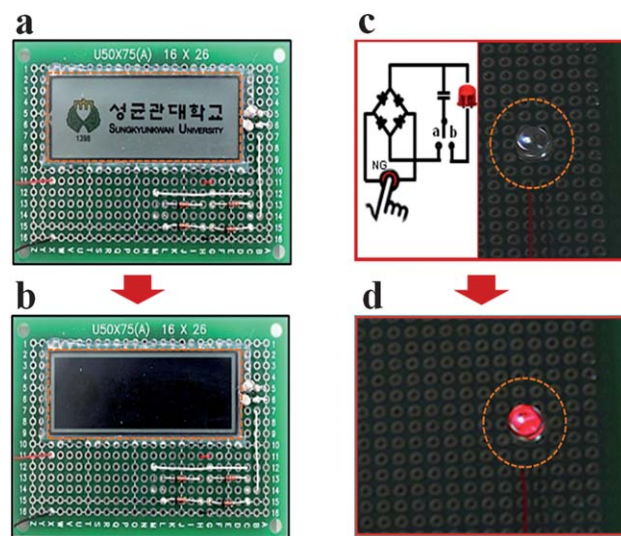


**Fig. 6** LCD and LED application of the electric energy generated by the nanogenerator to drive a commercial liquid crystal display and a light emitting diode. (a) Images of the Sungkyunkwan University logo on an LCD and (b) after it was turned on by the nanogenerator. (c) Image of a commercial LED, which is incorporated into the circuit in dim background before it was lit up. (d) Image of the LED in dim background at the moment when it was lit up by the PZT nanogenerator.

inside the LCD screen changes in response to electrical charges, therefore LCDs could be run by the electrical charges generated from the NGs under periodic stress. It was observed that the LCD screen can continuously turn 'ON' with the as-fabricated PZT NGs output power, indicating their good and stable performance. The LCD screen can be regarded as a capacitive device, as the liquid crystal is sandwiched between the two electrode plates. When the LCD screen is connected to the output of PZT NGs, it stores the charges. The stored charges start to release when one output pulse from NGs vanishes, and until the next output pulse comes. But continuous lighting of the LCD screen is only possible if, during this time interval, the electric field created by the remaining stored charges exceeds the threshold voltage of the screen. To demonstrate another practical application using PZT NGs, the LED was lit up with their output power using a charging–discharging electrical circuit in two steps, as shown in the inset of Fig. 6c. In the first step, the output of PZT NGs was connected to a full wave rectifying circuit comprising four diodes, and then the capacitor ( $22 \mu\text{F}$ ) was charged with fully rectified signals by pressing the switch 'A'. In the second step, when the capacitor was saturated it was then used to derive the LED by closing the switch 'B'. Fig. 6c and d show photographs of the LED before and after it was lit up.

#### 4. Conclusions

In summary, we demonstrated high performance PZT NGs using transparent graphene as interdigitated electrodes. The extraordinary mechanical, optical and electrical properties of graphene were exploited in the fabrication of PZT NGs. For realizing the practical use of NGs, we successfully drove the LCD screen and LED with the output power of PZT NGs. The results presented here may create new possibilities for energy

harvesting systems, particularly in applications that require flexibility and semi-transparency.

## Acknowledgements

This research was supported by the Basic Research Program and Global Frontier Research Center for Advanced Soft Electronics through the National Research Foundation of Korea (NRF), funded by the Ministry of Education, Science and Technology (2011-0006268, 2009-0064888, 2011-0030014 and 2012006049), the Research Centre of Breakthrough Technology Program through the Korea Institute of Energy Technology Evaluation and Planning (KETEP), funded by the Ministry of Knowledge Economy (MKE) (2009-3021010030-11-1), and the Energy International Collaboration Research & Development Program of the KETEP funded by the MKE (2011-8520010050).

## References

- 1 C. Sun, J. Shi and X. Wang, *J. Appl. Phys.*, 2010, **108**, 034309.
- 2 J. H. Jung, M. Lee, J. I. Hong, Y. Ding, C. Y. Chen, L. J. Chou and Z. L. Wang, *ACS Nano*, 2011, **5**, 10041.
- 3 L. E. Cross, *Nature*, 2004, **432**, 24.
- 4 Y. Saito, H. Takao, T. Tani, T. Nonoyama, K. Takatori, T. Homma, T. Nagaya and M. Nakamura, *Nature*, 2004, **432**, 84.
- 5 Z. Wang, J. Hu, A. P. Suryavanshi, K. Yum and M. F. Yu, *Nano Lett.*, 2007, **7**, 2966.
- 6 (a) S. Xu, B. J. Hansen and Z. L. Wang, *Nat. Commun.*, 2010, **1**, 93; (b) Y. Qi and M. C. McAlpine, *Energy Environ. Sci.*, 2010, **3**, 1275; (c) C. Sun, J. Shi, D. J. Bayerl and X. Wang, *Energy Environ. Sci.*, 2011, **4**, 4508.
- 7 Y. Hu, Y. Zhang, C. Xu, L. Lin, R. L. Snyder and Z. L. Wang, *Nano Lett.*, 2011, **11**, 2572.
- 8 R. Yang, Y. Qin, L. Dai and Z. L. Wang, *Nat. Nanotechnol.*, 2009, **4**, 34.
- 9 C. Y. Chen, J. H. Huang, J. Song, Y. Zhou, L. Lin, P. C. Huang, Y. Zhang, C. P. Liu, J. H. He and Z. L. Wang, *ACS Nano*, 2011, **5**, 6707.
- 10 K. H. Kim, K. Y. Lee, J. S. Seo, B. Kumar and S. W. Kim, *Small*, 2011, **7**, 2577.
- 11 J. Liu, P. Fei, J. Zhou, R. Tummala and Z. L. Wang, *Appl. Phys. Lett.*, 2008, **92**, 173105.
- 12 C. T. Huang, J. Song, W. F. Lee, Y. Ding, Z. Gao, Y. Hao, L. J. Chen and Z. L. Wang, *J. Am. Chem. Soc.*, 2010, **132**, 4766.
- 13 L. Lin, C. H. Lai, Y. Hu, Y. Zhang, X. Wang, C. Xu, R. L. Snyder, L. J. Chen and Z. L. Wang, *Nanotechnology*, 2011, **22**, 475401.
- 14 X. Wang, J. Song, F. Zhang, C. He, Z. Hu and Z. L. Wang, *Adv. Mater.*, 2010, **22**, 2155.
- 15 Y. F. Lin, J. Song, Y. Ding, S. Y. Lu and Z. L. Wang, *Appl. Phys. Lett.*, 2008, **92**, 022105.
- 16 Y. F. Lin, J. Song, Y. Ding, S. Y. Lu and Z. L. Wang, *Adv. Mater.*, 2008, **20**, 3127.
- 17 G. Zhu, R. Yang, S. Wang and Z. L. Wang, *Nano Lett.*, 2010, **10**, 3151.
- 18 F. Fan, Z. Tian and Z. L. Wang, *Nano Energy*, 2012, **1**, 328.
- 19 Yi. Qi, N. T. Jafferis, K. Lyons Jr, C. M. Lee, H. Ahmad and M. C. McAlpine, *Nano Lett.*, 2010, **10**, 524.
- 20 Y. Qi, J. Kim, T. D. Nguyen, B. Lisko, P. K. Purohit and M. C. McAlpine, *Nano Lett.*, 2011, **11**, 1331.
- 21 K. Park, S. Xu, Y. Liu, G. T. Hwang, S. L. Kang, Z. L. Wang and K. J. Lee, *Nano Lett.*, 2010, **10**, 4939.
- 22 J. G. E. Gardeniers, A. Smith and C. Cobianu, *J. Microchem. Microeng.*, 1995, **5**, 153.
- 23 N. Izyumskaya, Y.-I. Alivov, S.-J. Cho, H. Morkoc, H. Lee and Y. S. Kang, *Crit. Rev. Solid State Mat. Sci.*, 2007, **32**, 111.
- 24 B. Noheda, D. E. Cox, G. Shirane, R. Guo, B. Jones and L. E. Cross, *Phys. Rev. B: Condens. Matter Mater. Phys.*, 2000, **63**, 014103.
- 25 X. Chen, S. Y. Xu, N. Yao, W. H. Xu and Y. Shi, *Appl. Phys. Lett.*, 2009, **94**, 253113.
- 26 L. M. Swallow, J. K. Luo, E. Siores, I. Patel and D. Dodds, *Smart Mater. Struct.*, 2008, **17**, 025017.
- 27 S. Bae, H. Kim, Y. Lee, X. Xu, J. S. Park, Y. Zheng, J. Balakrishnan, T. Lei, H. R. Kim, Y. I. Song, Y. J. Kim, K. S. Kim, B. Ozyilmaz, J. H. Ahn, B. H. Hong and S. Iijima, *Nat. Nanotechnol.*, 2010, **5**, 574.
- 28 X. Chen, S. Xu, N. Yao and Y. Shi, *Nano Lett.*, 2010, **10**, 2133.